ACS EARTH AND SPACE CHEMISTRY

http://pubs.acs.org/journal/aesccq

Article

Diffusional Isotope Effect Based on the Transition-State Theory of Interstitial Mechanism in Solids

Xuefang Li,[‖] Yining Zhang,[‖] and Yun Liu*

Cite This: *ACS Earth Space Chem.* 2023, 7, 28−40

Read Online

ACCESS | Metrics & More | Article Recommendations | Supporting Information

ABSTRACT: It is important to be able to interpret the rapidly growing isotopic diffusion data in mineral grains that are measured using high spatial resolution. Based on previous works, the classical transition-state theory, and quantum statistical mechanics, an atomic theory to evaluate the diffusion coefficient (D) and the kinetic isotope effect (β factor) for the interstitial diffusion mechanism is developed with the unified equations for theoretical calculations. Taking helium diffusion in forsterite as an example, the D and β ($^4He/^3He$) were calculated at certain upper mantle conditions (0−20 GPa, 0−1500 °C) based on the developed equations. All parameters needed in our theory were obtained by first-principles calculations. Our calculated results for D at 0 GPa show reasonable agreement with most experimental results, indicating acceptable validity of the developed theory and methods. Meanwhile, possible causes for slight differences between calculations and experimental results at ambient pressure were also explored. We find that the β increases with the increase of temperature, but its pressure dependence is quite limited at least in the case of interstitial helium diffusion in forsterite. Additionally, we confirmed that current widely used simulation protocols with a fixed lattice for diffusion fail to accurately estimate the D values under high pressures due to the neglection of the activation volume. However, we also find that such protocols have almost negligible effects on the β factors for isotope fractionations during diffusion. Finally, potential effects of various approximations and calculation protocols involved in previous studies were carefully evaluated, and we find that some commonly used approximations and techniques are oversimplified and probably lead to significant loss of accuracy, especially at low temperatures (≤~600 °C). However, it is still quite safe to continue adopting these protocols when dealing with high-temperature problems (e.g., ≥1000 °C).

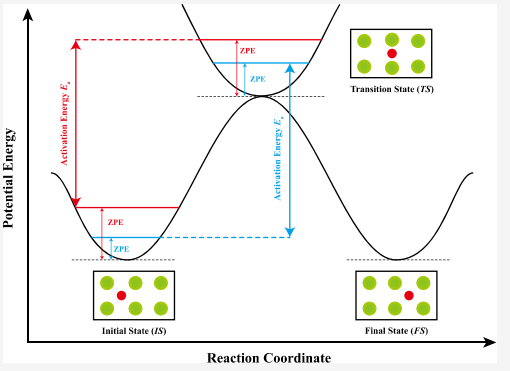

KEYWORDS: *interstitial diffusion, isotope effect, transition-state theory, first-principles calculations, helium diffusion, forsterite*

1. INTRODUCTION

Diffusion is one of the most important ways to transfer matter in solids. The study of diffusion in solids can provide information about the spatial scale of distribution and migration time of trace elements and isotopes in mineral grains and surrounding media,[1−3] reflecting detailed thermal history and growth of minerals.[4] It can also be used to quantitatively estimate closure temperatures of element and isotope diffusions in minerals.[5,6] Therefore, quantification of the diffusional isotope effect (DIE) is a key to tracing processes that can be widely applied in isotope geochemistry, high-temperature petrology, chemical geodynamics, cosmochemistry, and thermochronology.

The DIE can cause large isotope fractionations and produce unique isotope zoning fingerprints in mineral grains.[7,8] For example, Li isotope diffusion within minerals or grain boundaries has been confirmed to affect Li isotope distribution;[9−13] Fe and Ni isotopes were found fractionated in iron meteorites, which were attributed to diffusion;[14,15] Mg and Fe isotope composition profiles in zoned olivine were also attributed to diffusion.[7,16−20]

The molecular level mechanism of isotopic fractionation is crucial for accurate quantifications of those profiles. An accurate theoretical framework accompanied with reasonable calculation methods of DIE is a prerequisite for applications of this powerful tracer.

In the 1950s, based on the theory of absolute reaction rate via a transition state,[21] the diffusion coefficient for interstitial atoms[23,24] and the isotope effect in solids were explored.[25] These pioneering works were all based on the classical transition-state theory (CTST). Subsequent studies showed that the ratio of diffusion coefficient for two isotopes is inversely proportional to the square root ratio of isotope masses[26,27] when the correlation coefficient f is 1. Later, this relationship was further modified by introducing the coupling

Received: April 20, 2022
Revised: November 21, 2022
Accepted: November 23, 2022
Published: December 7, 2022

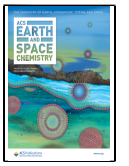

coefficient K.[28,29] Moreover, the diffusion-controlled thermal gradient effect in silicate melts, that is, the Soret effect, was studied theoretically.[30,31] In 2015, the theory and calculation of DIE were carefully reviewed and showed that it depends on the product of f and K.[32]

Recently, many researchers have started to use the first-principles quantum chemistry methods to calculate diffusion coefficients of elements in mantle minerals.[33−37] Specifically, Wang et al.[36] calculated interstitial diffusion of helium (He) in forsterite and checked its temperature and pressure dependences. Their results suggested that the migration distance of He during 1 million years is about 2.7 m at upper mantle conditions. Wang et al.[37] investigated the recycling of noble gases by calculating the diffusions of noble gases, that is, He, Ne, Ar, Kr, and Xe, in subduction materials. They found that oceanic crust and the lithospheric mantle of the subduction slab play different roles in delivering noble gases into the mantle.

However, previous calculations were all based on the theoretical frameworks established around 1950s to 1960s in the field of solid-state physics. Many approximations, such as the one-atom model[23,24] and the high-temperature approximation,[25,29] were used in previous works without careful and systematic validations. These theoretical treatments may be no longer meeting the required precision for the calculation of DIE nowadays.

Here, we provide an improved theory of the DIE for interstitial diffusion processes in solids based on the CTST. In addition, the validity and accuracy of this new framework are carefully checked through first-principles calculations of interstitial diffusion of helium in forsterite at different temperatures and pressures.

2. THEORY AND METHODS

2.1. Microscopic Expression of *D*. From a microscopic viewpoint, diffusion occurs by successive atomic jumps in a crystal lattice; the microscopic expression of diffusion coefficient (D) is[38]

$$D = \alpha f d^2 \Gamma \tag{1}$$

where α is the geometric factor, whose value depends upon the location of defects (interstitials or vacancies), f is the correlation coefficient[39] denoting the degree of correlation between successive jumps, d is the jump distance for one atomic jump step during diffusion, and Γ is the atomic jump frequency (number of jumps per unit time) from one site to the neighboring site. For the interstitial mechanism explored in this study, f equals 1, which means that there are no correlations between successive jumps. Therefore, accurately obtaining the value of Γ is the key to calculating the D of interstitial diffusion.

2.2. Previous Studies about Γ. Based on the CTST developed by Eyring,[21] the diffusion process was modeled as a reaction where the solute atom has to be activated and overcome an energy barrier from one site of energy minimum to a saddle point (the transition state) and further reach the neighboring energy minimal position.[23,24] According to this model, Wert and Zener[23] and Wert[24] developed the following equation for Γ

$$\Gamma = n\nu\, e^{\Delta S/R}\, e^{-E/RT} = \frac{k_B T}{h} n'\, e^{\Delta S^*/R}\, e^{\Delta H^*/RT} \tag{2}$$

where n is the number of the closest neighboring interstitial sites, ν is the vibration frequency of a solute atom in an interstitial site, $e^{\Delta S/R}$ is the entropy factor, E is the heat of activation, n' is the number of equivalent pathways of diffusion from a given lattice site, ΔS^* and ΔH^* are the corresponding entropy and heat of activation, respectively, R is the ideal gas constant, T is the temperature in kelvin, h is the Planck constant, and k_B is the Boltzmann constant. The commonly used activation energy can be expressed as $(E - T\Delta S)$ or $(\Delta H^* - T\Delta S^*)$.

However, Vineyard[25] pointed out that eq 2 was oversimplified by using the one-atom model to deal with the diffusion, which only considered the vibration of the solute atom in the direction of the saddle point; meanwhile, the vibrations of other atoms were all fixed. By ignoring all the quantum effects and treating all the motions near the saddle point as harmonic oscillators, combining the classical statistical mechanics, Vineyard[25] developed a new equation which includes the many-body effect caused by vibrations of surrounding atoms of the solute atom

$$\Gamma = \tilde{\nu}\, e^{-\Delta E/k_B T} \tag{3}$$

where $\tilde{\nu}$ is called the effective frequency and ΔE is the potential energy difference between the initial equilibrium site and the one at the saddle point. The value of $\tilde{\nu}$ is further expressed as

$$\tilde{\nu} = \prod_{j=1}^{3N} \nu_j \Big/ \prod_{j=1}^{3N-1} \nu_j' \tag{4}$$

where N is the total number of atoms in the system, ν_j is the harmonic vibration frequency of the system at the initial site, ν_j' is the frequency of the system constrained at the saddle point, and "$3N - 1$" means that the vibration frequency in the direction of the saddle point is excluded. Furthermore, Le Claire[29] estimated the quantum effects at high temperatures and modified eq 3 into

$$\Gamma = \frac{k_B T}{h} \left(\prod_{j=1}^{3N-1} \frac{e^{-h\nu_j'/2k_B T}}{e^{-h\nu_j/2k_B T}} \frac{1 - e^{-h\nu_j/k_B T}}{1 - e^{-h\nu_j'/k_B T}} \right) e^{-\Delta E/k_B T} \tag{5}$$

2.3. Previous Studies of DIE for Interstitial Diffusion. According to eq 1, the ratio of the two Ds for heavy and light isotopes is equal to the ratio of two Γs because α and a for different isotopes are the same under the widely used Born−Oppenheimer approximation (BOA) framework.[40] According to eq 2, Schoen[26] proposed that the ratio of Ds for two isotopes is inversely proportional to the square root ratio of isotope masses

$$\frac{D^*}{D} = \frac{\Gamma^*}{\Gamma} = \sqrt{\frac{m}{m^*}} \tag{6}$$

where m is the atomic mass and "*" denotes the one involving the heavy isotope. However, Mullen[28] found that eq 6 failed to match the experimental data of ^{55}Fe and ^{59}Fe in pure crystals of silver and copper and proposed that eq 6 should be modified into

$$\frac{D^*}{D} - 1 = \Delta K \left(\sqrt{\frac{m}{m^*}} - 1 \right) \tag{7}$$

where the ΔK was described as the fraction of the translational kinetic energy which is possessed by the solute atom as it crosses the saddle point. Le Claire[29] also gave an alternative

https://doi.org/10.1021/acsearthspacechem.2c00110
ACS Earth Space Chem. 2023, 7, 28−40

derivation of eq 7 and discussed the physical meaning of ΔK in terms of the lattice vibration and proposed that quantum corrections to the classical rate equations for atomic jump frequencies are important for the diffusion of light interstitial solutes such as H_2 and D_2. In 2015, Van Orman and Krawczynski[32] rewrote the "ΔK" as "K" (we also use "K" instead of "ΔK" in this article) and summarized that the ratio of the diffusion coefficients for two isotopes depends on the product of f and K

$$\frac{\frac{D^*}{D}-1}{\left(\frac{m}{m^*}\right)^{1/2}-1} = E = fK \approx \frac{\ln\left(\frac{D^*}{D}\right)}{ln\left(\sqrt{\frac{m}{m^*}}\right)} \tag{8}$$

and they quantitatively estimated the isotope effects for several cations in periclase, olivine, magnetite, and rutile.

Additionally, researchers also use another equation to evaluate the magnitude of isotope fractionation during diffusion,[41−44] where the ratio of two Ds is connected to the mass ratio of two isotopes by the exponent β as

$$\frac{D^*}{D} = \left(\frac{m}{m^*}\right)^{\beta} \tag{9}$$

β is also known as the diffusional kinetic isotope fractionation factor, and it has often been used to evaluate the relative diffusivity of isotopes in recent studies.[44,45]

2.4. Calculation of Γ. By analyzing these previous works, we developed the theory to treat the atomic jump in interstitial diffusion processes based on CTST[21,46] and quantum statistical mechanics. We treat interstitial diffusion process as a set of atomic jump steps, and each step can be modeled as an elementary reaction in which the solute atom jumps from one interstitial equilibrium site (denoted as initial state, IS) to a neighboring one (denoted as final state, FS) by overcoming an energy barrier and crossing the saddle point (transition state, TS). The CTST always assumes a quasi-equilibrium between IS and TS.[37] Like the CTST, the atomic jump step from IS to FS can be expressed as (the unidirectional scenario)

$$\mathrm{IS} \xrightarrow{K_{eq}} \mathrm{TS} \xrightarrow{\nu^{\neq}} \mathrm{FS} \tag{10}$$

where we assume quasi-equilibrium (both chemical and isotopic) between IS and TS with an equilibrium constant of K_{eq}, and TS can directly dissociate into FS through vibration ($\nu^{\neq}$) along the direction of jump. Therefore, the reaction rate r of the jump step can be expressed as

$$r = \frac{\mathrm{d[FS]}}{\mathrm{d}t} = \nu^{\neq}[\mathrm{TS}] \tag{11}$$

where [IS] and [TS] denote the concentrations of IS and FS. As for the fate of TS, we can also assume that TS can form both FS in a forward direction and IS in a reversed direction. This will not affect the results in terms of ratio for different isotopes. Based on the quasi-equilibrium assumption between IS and TS, we thus have

$$K_{eq} = \frac{[\mathrm{TS}]}{[\mathrm{IS}]} \tag{12}$$

and

$$r = \nu^{\neq}K_{eq}[\mathrm{IS}] \tag{13}$$

Based on eqs 1 and 13 and combining the first Fick's law of diffusion, we have

$$\Gamma = \nu^{\neq}K_{eq} \tag{14}$$

Detailed derivations of eq 14 are summarized in Supporting Information S1. Starting from eq 14, K_{eq} under certain temperatures and pressures can be expressed in a thermodynamic function form as

$$K_{eq} = \mathrm{e}^{-\Delta G/k_BT} = \mathrm{e}^{-\Delta F+P\Delta V/k_BT} = \mathrm{e}^{-\Delta F/k_BT}\,\mathrm{e}^{-P\Delta V/k_BT} \tag{15}$$

where ΔG and ΔF are the Gibbs and Helmholtz free-energy differences between the TS and IS, respectively, and ΔV is the activation volume for the interstitial diffusion process. According to molecular thermodynamics, we can rewrite eq 15 by introducing the partition function (q) as

$$F = -k_BT\ \ln q \tag{16}$$

$$K_{eq} = \frac{q_{TS}}{q_{IS}}\,\mathrm{e}^{-P\Delta V/k_BT} \tag{17}$$

where q_{IS} and q_{TS} are the total partition functions of IS and TS, respectively. For crystals, the total partition function q can be further expressed as

$$q = q_{elec}\cdot q_{vib} \tag{18}$$

where q_{elec} and q_{vib} are the electronic and vibrational partition functions, respectively. Assuming that the lattice vibrations are harmonic, we have

$$\begin{aligned} K_{eq} &= \frac{(q_{elec}\cdot q_{vib})_{TS}}{(q_{elec}\cdot q_{vib})_{IS}}\,\mathrm{e}^{-P\Delta V/k_BT} \\ &= \frac{\left(\prod_{i=1}^{3N}\frac{\mathrm{e}^{-u_i/2}}{1-\mathrm{e}^{-u_i}}\right)_{TS}}{\left(\prod_{i=1}^{3N}\frac{\mathrm{e}^{-u_i/2}}{1-\mathrm{e}^{-u_i}}\right)_{IS}}\,\mathrm{e}^{-\Delta E_{elec}/k_BT}\,\mathrm{e}^{-P\Delta V/k_BT} \end{aligned} \tag{19}$$

where ΔE_{elec} is the electronic energy difference between TS and IS, $u_i = \frac{h\nu_i}{k_BT}$, and ν_i is the harmonic vibration frequency of the i-th normal mode. Then we obtain the expression for Γ as

$$\Gamma = \nu^{\neq}\frac{\left(\prod_{i=1}^{3N}\frac{\mathrm{e}^{-u_i/2}}{1-\mathrm{e}^{-u_i}}\right)_{TS}}{\left(\prod_{i=1}^{3N}\frac{\mathrm{e}^{-u_i/2}}{1-\mathrm{e}^{-u_i}}\right)_{IS}}\,\mathrm{e}^{-\Delta E_{elec}/k_BT}\,\mathrm{e}^{-P\Delta V/k_BT} \tag{20}$$

This is the initial equation for calculating the jump frequency without any extra approximations or simplifications. For the two items involving the vibration frequency in eq 20, if we separate the $\nu^{\neq}$ mode from the q_{vib} of the TS and using the following high-temperature approximation

$$h\nu \ll k_BT \tag{21}$$

Equation 20 can be simplified by using the first-order approximation of Taylor expansion into

https://doi.org/10.1021/acsearthspacechem.2c00110
ACS Earth Space Chem. 2023, 7, 28−40

$$\Gamma = \nu^{\neq}\frac{1-\frac{h\nu^{\neq}}{2k_BT}}{1-\left(1-\frac{h\nu^{\neq}}{k_BT}\right)}\frac{\left(\prod_{i=1}^{3N-1}\frac{e^{-u_i/2}}{1-e^{-u_i}}\right)_{TS}}{\left(\prod_{i=1}^{3N}\frac{e^{-u_i/2}}{1-e^{-u_i}}\right)_{IS}}e^{-\Delta E_{elec}/k_BT}$$

$$e^{-P\Delta V/k_BT} \approx \frac{k_BT}{h}\frac{\left(\prod_{i=1}^{3N-1}\frac{e^{-u_i/2}}{1-e^{-u_i}}\right)_{TS}}{\left(\prod_{i=1}^{3N}\frac{e^{-u_i/2}}{1-e^{-u_i}}\right)_{IS}}e^{-\Delta E_{elec}/k_BT}$$

$$e^{-P\Delta V/k_BT} = \frac{k_BT}{h}\frac{q'_{TS}}{q_{IS}}e^{-\Delta E_{elec}/k_BT}e^{-P\Delta V/k_BT} \quad (22)$$

We notice that eq 22 is actually the commonly used equation eq 5 that was proposed by Le Claire[29] for calculating Γ. However, it is worth mentioning that for the vibrational part of the total partition function of transition state (q'_{TS}), it includes only $3N-1$ rather than $3N$ degrees of freedom, and this equation shall not be used unless eq 21 is well satisfied.[47] If eq 20 is further simplified by assuming that all the vibration frequencies satisfy the conditions used in eq 21, then we can obtain the following expression for Γ

$$\Gamma \approx \frac{\left(\prod_{i=1}^{3N}\nu_j\right)_{IS}}{\left(\prod_{i=1}^{3N-1}\nu_j\right)_{TS}}e^{-\Delta E_{elec}/k_BT}e^{-P\Delta V/k_BT} \quad (23)$$

Here, we can see that the zero-point vibrational energy difference (ΔZPE) between TS and IS has been completely neglected with this approximation. However, when it comes to the DIE, such an approximation will lead to large errors due to the well-known fact that the ΔZPE is one of the most important driving forces for isotope fractionation.

Interestingly, eq 23 is very similar to eq 3, which was developed by Vineyard (1957) using the classic statistical mechanics combined with the CTST. Now we know that eq 23 is actually an approximated form of eq 20 by assuming $h\nu \ll k_BT$ for all the vibrational modes. In other words, eq 23 can only be applied to high-temperature cases. Unfortunately, most previous studies calculated Γ by directly using the equation of Vineyard[25] without considering whether eq 21 is satisfied or not.[36,37,48,49] We show in Section 4 that this will lead to significant errors for both D and ratio of two Ds of heavy and light isotopes at relatively low temperatures.

2.5. Calculation of $\frac{D^*}{D}$. Figure 1 shows the potential energy profiles of one atomic jump step involving the heavy and light isotopes during the interstitial diffusion process. Note that the activation energy for the light isotope is smaller than the one for the heavy isotope. Based on our derived equations (e.g., eq 20), the ratio of two Ds of heavy (D^*) and light isotopes (D) can be expressed as

$$\frac{D^*}{D} = \frac{\Gamma^*}{\Gamma} = \frac{\nu^{\neq,*}}{\nu^{\neq}}\frac{\left(\prod_{i=1}^{3N}\frac{e^{-u_i^*/2}}{e^{-u_i/2}}\frac{1-e^{-u_i}}{1-e^{-u_i^*}}\right)_{TS}}{\left(\prod_{i=1}^{3N}\frac{e^{-u_i^*/2}}{e^{-u_i/2}}\frac{1-e^{-u_i}}{1-e^{-u_i^*}}\right)_{IS}}e^{-\Delta\Delta E_{elec}/k_BT}e^{-P\Delta\Delta V/k_BT} \quad (24)$$

This is the unified equation for calculating DIE we derived, and it can be applied to any interstitial diffusion systems in the future. Here, $\Delta\Delta E_{elec}$ and $\Delta\Delta V$ are the differences of ΔE_{elec} and ΔV between the heavy and light isotopes. For example, $\Delta\Delta E_{elec} = (E^*_{elec} - E_{elec})_{TS} - (E^*_{elec} - E_{elec})_{IS}$.

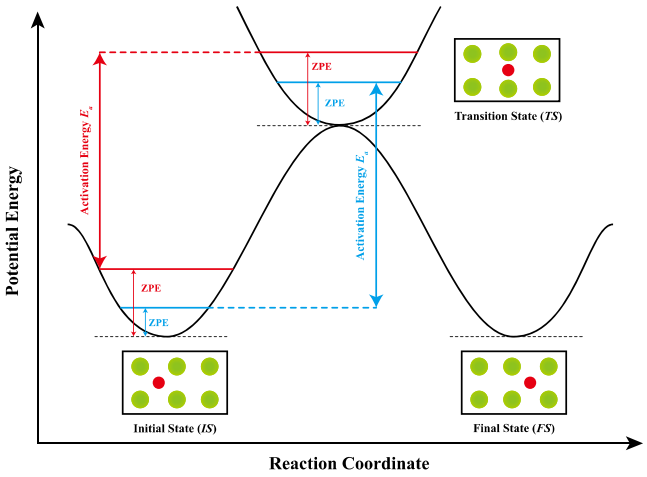

Figure 1. Schematic diagram of the potential energy profile along the reaction coordinate for one elementary atomic jump step during the interstitial diffusion process. The blue line denotes the process involving the heavy isotope, and the red line denotes the one involving light isotopes.

Note that under the framework of BOA,[40] ΔE_{elec} and ΔV can be canceled and eq 25 will only have the terms associated with vibrations as follows

$$\frac{D^*}{D} = \frac{\nu^{\neq,*}}{\nu^{\neq}}\frac{\left(\prod_{i=1}^{3N}\frac{e^{-u_i^*/2}}{e^{-u_i/2}}\frac{1-e^{-u_i}}{1-e^{-u_i^*}}\right)_{TS}}{\left(\prod_{i=1}^{3N}\frac{e^{-u_i^*/2}}{e^{-u_i/2}}\frac{1-e^{-u_i}}{1-e^{-u_i^*}}\right)_{IS}} \quad (25)$$

Issues beyond the BOA framework will be briefly discussed in Section 4.4.

If we adopt the high-temperature approximation for $\nu^{\neq}$ (eq 21), then we have the first approximation of eq 24 denoted as AP1

$$\text{AP1: } \frac{D^*}{D} \approx \frac{\left(\prod_{i=1}^{3N-1}\frac{e^{-u_i^*/2}}{e^{-u_i/2}}\frac{1-e^{-u_i}}{1-e^{-u_i^*}}\right)_{TS}}{\left(\prod_{i=1}^{3N}\frac{e^{-u_i^*/2}}{e^{-u_i/2}}\frac{1-e^{-u_i}}{1-e^{-u_i^*}}\right)_{IS}} \quad (26)$$

Then if we further use the same approximation for the other vibrational modes, we can obtain the second approximation denoted as AP2

$$\text{AP2: } \frac{D^*}{D} \approx \frac{\left(\prod_{i=1}^{3N}\frac{\nu_i^*}{\nu_i}\right)_{IS}}{\left(\prod_{i=1}^{3N-1}\frac{\nu_i^*}{\nu_i}\right)_{TS}} \quad (27)$$

2.6. First-Principles Density Functional Theory Calculations. Interstitial diffusion of He in forsterite is used here as an example to evaluate the validity of our newly developed theoretical framework and calculation methods. All parameters needed in eqs 20 and 25 are obtained using the first-principles calculations based on density functional theory, which is implemented in the Vienna ab initio simulation package (VASP, version 5.3.3).[50,51] The transition states are located using the climbing image nudged elastic band (CI-NEB)

https://doi.org/10.1021/acsearthspacechem.2c00110
ACS Earth Space Chem. 2023, 7, 28−40

method.[52−54] The CI-NEB method is a modified version of the nudged elastic band method (NEB). The NEB method locates the saddle point by constructing a set of images between the IS and the FS; that is, the starting geometric configuration of each image is directly constructed as the incremental intermediate between the IS and FS. By adding pseudo spring forces between each image and decomposing the true forces and the pseudo spring forces into two components (parallel and perpendicular to the reaction path), the reaction path can be optimized by minimizing the forces acting on each image.[53] However, the NEB method often uses the same spring force constants between neighboring images. Thus, typically, none of the images can actually be located at or near the true saddle point, and a further interpolation scheme must be performed to estimate the position and energy of the saddle point.[53] To further improve the robustness of the optimization, the CI-NEB method was developed to avoid this problem by further identifying the image with the maximum force and allowing it to move along the reaction path and ensure that it reaches the actual maxima. Therefore, CI-NEB ensures a rigorous convergence for locating the saddle point, and we decided to use this method to search the TS for the interstitial diffusion of helium in forsterite.

The interactions between ions and electrons are handled using the projected augmented wave method[55,56] using pseudopotentials implemented in VASP's pseudopotential library. The valence electronic configurations used in our calculations are Mg ($3s^2 3p^0$), Si ($3s^2 3p^2$), O ($2s^2 2p^4$), and He ($1s^2$). The functional proposed by Perdew and Wang (PW91)[57] is used to describe the exchange and correlation energy between electrons. The plane-wave energy cutoff is set to 600 eV for all calculations. For forsterite, the initial structure is extracted from data obtained by Fujino[58] with lattice parameters of a = 4.75 Å, b = 10.19 Å, and c = 5.98 Å and has been reoptimized before performing the CI-NEB calculations. Here, a 3 × 2 × 2 supercell (336 atoms in total) was employed with the space group of *Pbnm* that was checked by previous works of Wang et al.[36] for avoiding additional size effects. Such a supercell holds a minimum distance (along the c-axis) of 11.96 Å between two neighboring He atoms in two adjacent supercells, and the Coulombic interactions between them can be safely neglected (<4 kJ/mol).[36] The interstitial helium atom is located in a pre-searched interstitial site which is nearly in the middle of two Mg cations with minimum total energy. As for the CI-NEB calculations, we use the forsterite crystal with He impurity with all its lattice parameters (a, b, c, α, β, γ) being fixed and just optimize their atomic positions (denoted as fixation method). We believe that such fixation will lead to nonphysical zero values for the activation volume ΔV, potentially indicating the failure of such a method for accurately estimating D values under high pressures. Therefore, issues about this fixation method are discussed in detail later (Section 4.4).

3. RESULTS

3.1. Interstitial Diffusion of He in Forsterite. Consistent with the results of Wang et al.,[36] we find that the structure shown in Figure 2 is the one with minimum total energy (IS or FS site in Figure 1), where He atom is located at the middle of two Mg2 cations along the [100] (a-axis) direction. Vibrational frequency analyses are performed to confirm the validity of CI-NEB calculations for the transition states. Our results showed that there is only one imaginary frequency for each

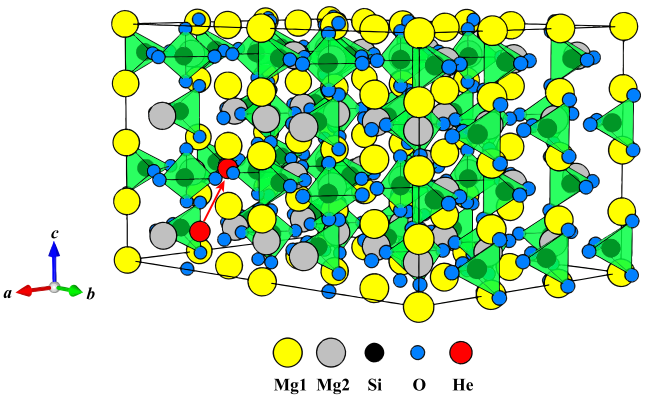

Figure 2. IS → FS atomic jump pathway of He atom in forsterite along the [101] direction (3 × 3 × 2 supercell). The jump pathway is denoted as a red arrow.

optimized saddle point configuration, indicating that the true transition state has been successfully located. The diffusion pathways we find are also consistent with the study of Wang et al.[36] The He atom jumps from one local minimum (IS) to a neighboring site (FS) by passing through a saddle point (TS) along the direction of [101] (Figure 2). Figure 3 shows the

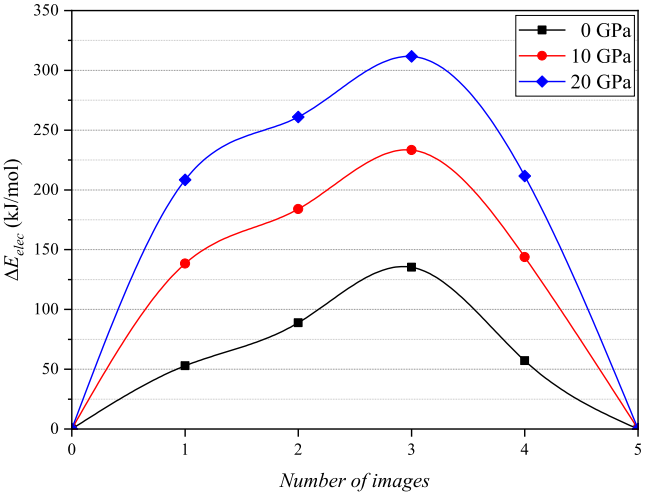

Figure 3. Calculated electronic energy profile for IS → FS pathways at 0, 10, and 20 GPa. The X-axis denotes the number of images in the CI-NEB calculations.

calculated potential energy profiles for IS → FS pathway of He interstitial diffusion in forsterite under different pressures. Four images were inserted from IS to FS configurations to search the transition states using the CI-NEB method. Our results showed that the third image corresponds to the highest potential energy along this reaction path, which is the transition state with the corresponding energy barrier ΔE_{elec} or E_a that was used by Wang et al.[36]

Based on the diffusion pathway identified and eq 1, we can determine that the net diffusion coefficient along the direction of [101] will be

$$D[101] = \frac{1}{2} d^2 \Gamma \tag{28}$$

Here, d is the jump distance of He atom from IS to FS (Table 1). The factor of 1/2 means that He atom can jump both forward and backward with the same probability. Using eq 20,

https://doi.org/10.1021/acsearthspacechem.2c00110
ACS Earth Space Chem. 2023, 7, 28−40

Table 1. Calculated Jump Distance of He from IS to FS (d), Fitted Pre-exponential Factor (D_0), and E_a of Diffusion in Arrhenius Form and R^2 of Fitting at 0, 10, and 20 GPa

P (GPa)	d (Å)	D_0(m^2/s)	E_a(kJ/mol)	R^2
0	4.0017	$4.94(6) \times 10^{-6}$	137.75(7)	0.999989
10	3.9065	$1.20(1) \times 10^{-6}$	236.13(7)	0.999997
20	3.8327	$2.12(1) \times 10^{-6}$	313.88(4)	0.9999995

we calculated the D values for ^{4}He from 0 to 1500 °C at 0, 10, and 20 GPa and plotted them in Figure 4. Figure 4 shows that

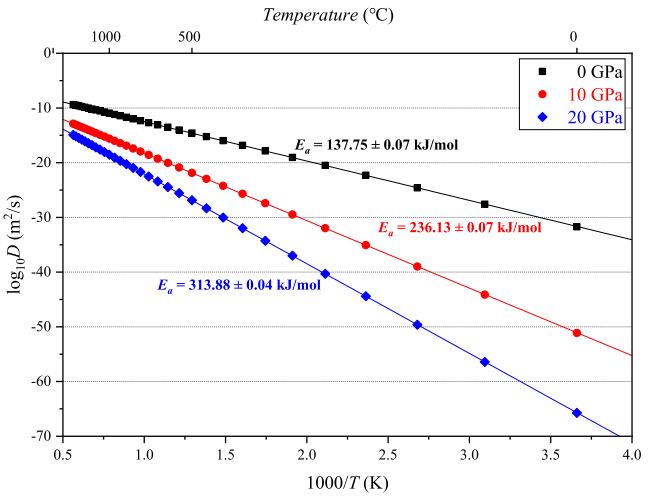

Figure 4. Calculated $\log_{10}D(^4\text{He})$ (m^2/s) vs 1000/T (K^{-1}) from 0 to 1500 °C at 0, 10, and 20 GPa. The fitted lines and corresponding E_a values are also plotted.

calculated $D[101](^4\text{He})$ values all follow the Arrhenius relationship. By fitting our results to the Arrhenius form of $D = D_0\, e^{-E_a/RT}$, we obtained both the pre-exponential factor D_0 and the activation energy of diffusion E_a as

$$0\ \text{GPa: } D[101](^4\text{He}) = 4.94(6) \times 10^{-6}\ \exp(-137.75(7)\ \text{kJ/mol/RT})\ \text{m}^2/\text{s}$$

$$10\ \text{GPa: } D[101](^4\text{He}) = 1.20(1) \times 10^{-6}\ \exp(-236.13(7)\ \text{kJ/mol/RT})\ \text{m}^2/\text{s}$$

$$20\ \text{GPa: } D[101](^4\text{He}) = 2.12(1) \times 10^{-6}\ \exp(-313.88(4)\ \text{kJ/mol/RT})\ \text{m}^2/\text{s}$$

The results in Table 1 show that E_a will significantly increase from 137.75(7) to 313.88(4) kJ/mol when the pressure increases from 0 to 20 GPa. Meanwhile, the jump distance (d) of He atom slightly decreases from 4.0017 Å at 0 GPa to 3.8327 Å at 20 GPa. In addition, $D[101](^4\text{He})$ will be significantly smaller under high pressures due to the greatly increased energy barrier E_a. For example, at 1000 °C, $D[101](^4\text{He})$ decreases from 1.11×10^{-11} m^2/s at 0 GPa to 2.83×10^{-19} m^2/s at 20 GPa with a variation of 8 orders of magnitude. This indicates that we may expect extremely slow interstitial diffusion of He in forsterite under high pressures, which seems quite intuitive. However, it is worth noting that the effect of the activation volume on D under high pressure is not considered here due to the fixation method, so the accuracy of Ds at 10 and 20 GPa here may be questionable. Additionally, although our calculated data of Ds at 10 and 20 GPa are probably problematic, it is still reasonable that they will not cause any trouble for evaluating the DIE in later sections, just as mentioned before in Section 2.5 (derivation of eq 25). More details and discussions about this problem are given in Section 4.4.

3.2. DIE of He Isotopes in Forsterite. For the IS → FS diffusion pathways of He in forsterite (Figures 2 and 3), we calculated the DIE in terms of both D^*/D and β using eqs 25 and 9 at certain upper mantle conditions, for example, the temperatures of 0−1500 °C and pressures of 0, 10, and 20 GPa (Table 2 and Figure 5).

Table 2. Calculated $\frac{D^*}{D}$ and β Values at 0, 10, and 20 GPa from 0 to 1500 °C

	0 GPa		10 GPa		20 GPa	
T (°C)	$\frac{D^*}{D}$	β	$\frac{D^*}{D}$	β	$\frac{D^*}{D}$	β
0	0.9831	0.0601	0.9908	0.0327	0.9864	0.0485
100	0.9431	0.2069	0.9506	0.1790	0.9501	0.1810
200	0.9205	0.2925	0.9270	0.2679	0.9279	0.2646
300	0.9069	0.3455	0.9122	0.3246	0.9136	0.3193
400	0.8981	0.3799	0.9026	0.3622	0.9041	0.3563
500	0.8921	0.4034	0.8960	0.3881	0.8975	0.3822
600	0.8879	0.4199	0.8913	0.4067	0.8928	0.4008
700	0.8849	0.4320	0.8879	0.4203	0.8893	0.4146
800	0.8826	0.4411	0.8853	0.4306	0.8867	0.4250
900	0.8809	0.4481	0.8833	0.4385	0.8846	0.4331
1000	0.8795	0.4536	0.8817	0.4448	0.8830	0.4395
1100	0.8785	0.4579	0.8805	0.4498	0.8818	0.4446
1200	0.8776	0.4615	0.8795	0.4538	0.8807	0.4488
1300	0.8769	0.4644	0.8786	0.4571	0.8799	0.4522
1400	0.8763	0.4668	0.8780	0.4599	0.8792	0.4551
1500	0.8758	0.4688	0.8774	0.4623	0.8786	0.4575

3.2.1. Temperature Effect. The results in Table 2 and Figure 5 show that D^*/D ratios are always less than 1, indicating that ^{3}He diffuses faster than ^{4}He in forsterite. Figure 5a shows that D^*/D ratio decreases as the temperature increases, meaning that we can expect greater DIEs under high temperatures. Similarly, Figure 5b shows that β increases with temperature, especially at the low-temperature range (0−1000 °C), and it gradually reaches 0.5 as the temperature increases. In addition, under the high-temperature range (≥1000 °C), the increase of β becomes quite limited. For example, at 0 GPa, β increases from 0.0601 to 0.4536 when the temperature increases from 0 to 1000 °C. However, β only changes from 0.4536 to 0.4688 when the temperature increases from 1000 to 1500 °C. When the temperature is extremely high (≥1500 °C), we can expect that β value will eventually converge to 0.5, which is the upper limit value of β and has been used for ideal gas diffusion in vacuum based on simple kinetic theory. It is quite interesting that β increases with increasing temperatures, although it seems a little bit counterintuitive as the ZPE should contribute more at lower temperatures (Figure 1). Actually, if we separate the β value into two parts, contributions from ZPE (denoted as β_{ZPE}) and the others (denoted as β_{others}), we can find that such a positive correlation between β and temperature is reasonable (Figure S1). For example, at 0 GPa, β_{ZPE} = −0.8088 and β_{others} = 0.8689 at 0 °C, and β_{ZPE} = −0.1246 and β_{others} = 0.5934 at 1500 °C (Supporting Information S2). Note

https://doi.org/10.1021/acsearthspacechem.2c00110
ACS Earth Space Chem. 2023, 7, 28−40

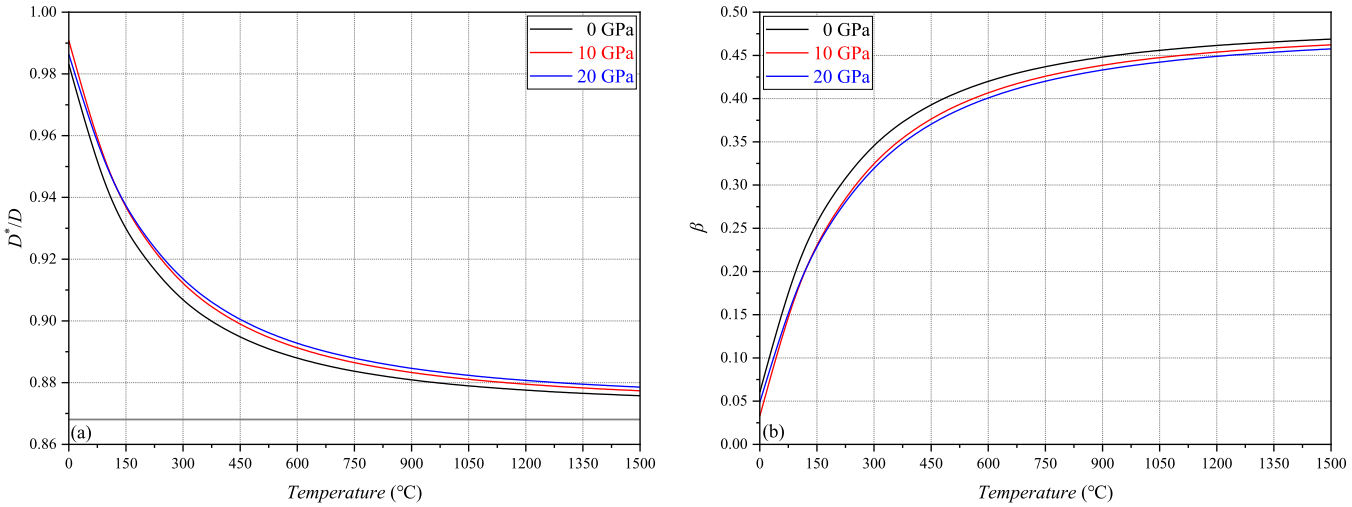

Figure 5. Calculated $\frac{D^*}{D}$ (a) and β (b) values from 0 to 1500 °C at 0, 10, and 20 GPa using eqs 9 and 25. The straight line in (a) shows the $\beta = 0.5$ limit for the $\frac{D^*}{D}$ ratio.

that the DIE is a kinetic isotope effect rather than an equilibrium isotope effect (EIE), so the ZPE shows a negative effect on the β values and such an effect will decrease as the temperature increases, which is intuitive from an EIE perspective. On the contrary, as the negative effect of ZPE decreases at high temperatures, the effect of β_{others} will become increasingly significant, which eventually causes such counter-intuitive temperature dependence of DIE.

3.2.2. Pressure Effect. Our results in Figure 5 show that the pressure effect on the D^*/D and β values is quite limited. Although the pressure has great effects on E_a and D, it seems that both light and heavy isotopes are affected to nearly the same extent, resulting in limited variations of the D^*/D and β values under different pressures. In this case, we find that β values will slightly decrease at high pressures.

In summary, the effects of pressure and temperature on the DIE are in opposite directions at least for this case. Stronger DIEs can be expected when temperatures are high at relatively low pressures. However, the temperature effect dominates, and the pressure effect is only significant for single D values but is trivial for DIE, that is, the ratio of two diffusion coefficients (D^*/D).

4. DISCUSSION

4.1. Comparison with Previous Results of D and E_a. Our calculated $D[101]$(^{4}He) values for interstitial diffusion of He in forsterite from 0 to 1500 °C at 0 GPa are compared with data obtained by previous experiments[22,59−65] and first-principles calculations[36] in Figure 6. As a small and uncharged atom, He commonly diffuses in minerals through an interstitial mechanism rather than vacancies.[66] A comparison of results in Figure 6 show that our calculated D values are slightly different from the values of some experiments and the first-principles calculations performed by Wang et al.[36] within 3 orders of magnitude, except for those of Hart[59] and Trull and Kurz.[22]

First, according to the Arrhenius form of D, that is, $D = D_0 \exp(-E_a/RT)$, the slopes of the lines in Figure 6 are directly related to the activation energy (E_a). Therefore, we can see that the slope of our calculations shows good agreement with the experimental data. The discrepancy of D is hence mainly caused by the D_0 part, that is, the pre-exponential factor, within

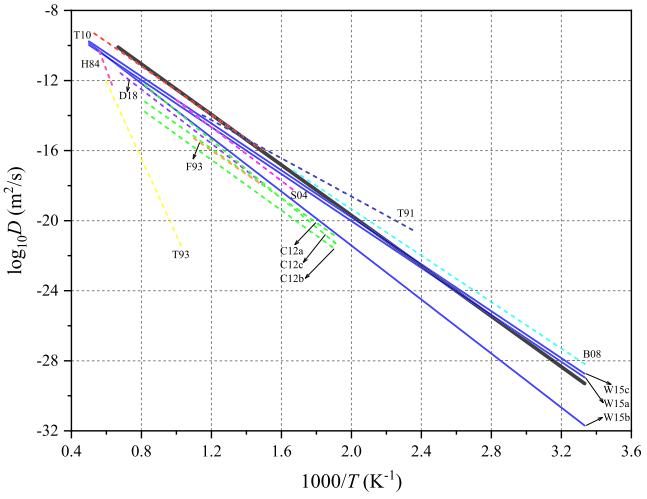

Figure 6. Comparison results between calculated $D(^4\text{He})[101]$ values from 0 to 1500 °C at 0 GPa with previous experimental and theoretical data. Data sources: H84;[59] T91;[60] F93;[61] T93;[22] S04;[62] B08;[63] T10;[64] C12;[66] W15;[36] D18.[65] Symbols *a*, *b*, and *c* for "C12" and "W15" represent diffusion directions along *a*-, *b*-, and *c*-axes, respectively. The bolded black line represents the data calculated in this study.

3 orders of magnitude of other experimental data. As for those significantly inconsistent results of Hart[59] and Trull and Kurz,[22] previous works have argued that those results were unrepresentative for the interstitial diffusion of He in olivine or forsterite.[65,66] Therefore, we decide to exclude those results and they will not be discussed in later sections. Compared with the results of Wang et al.,[36] our results show excellent agreements on D values along the *a*- and *c*-axes because we both hold the same diffusional pathway along the [101] direction. Additionally, differences on D values along the *b*-axis are mainly caused by diffusional pathway differences.

A detailed comparison of activation energy E_a is summarized in Table 3. Compared with experimental results, our fitted E_a value of 137.75(7) kJ/mol is generally in good agreement with most experimental results.[60−66] As for the smallest value obtained by Trull et al.,[60] considering the recently observed E_a

https://doi.org/10.1021/acsearthspacechem.2c00110
ACS Earth Space Chem. 2023, 7, 28−40

Table 3. Comparison of Calculated ΔE_{elec} and Fitted E_a Results between Our First-Principles Calculations and Previous Studies

P (GPa)	ΔE_{elec} (kJ/mol) this study	E_a(kJ/mol) this study	E_a(kJ/mol) previous studies
0	135.66	137.75(7)	148(49)[a], 128.33[b], 147.62[c], 135(5)[d], 138(13)[e], 159(4)[f], 133[g], 127(6)[h], 153.8(10)[i], 130(13)[j], 420(20)[k], 105(17)[l], 502(+134/−113)[m]
10	234.15	236.13(7)	156.31[b]
20	312.66	313.88(4)	not available

[a]Delon et al.,[65] D_{bulk}, step-heating experiments, polycrystalline olivine. [b]Wang et al.,[36] D[100] and D[001], theoretical calculations, Fo_{100}. [c]Wang et al.,[36] D[010], theoretical calculations, Fo_{100}. [d]Cherniak and Watson,[66] D[100], diffusion experiments, Fo_{100}. [e]Cherniak and Watson,[66] D[010], diffusion experiments, Fo_{100}. [f]Cherniak and Watson,[66] D[001], diffusion experiments, Fo_{100}. [g]Tolstikhin et al.,[64] D_{bulk}, release experiments, olivine in ultramafic rocks from Monche Pluton. [h]Blard et al.,[63] D_{bulk}, release experiments, San Carlos olivine, Fo_{92}. [i]Shuster et al.,[62] D_{bulk}, step-heating experiments, olivine from Guadalupe Island, Fo_{75-80}. [j]Futagami et al.,[61] D_{bulk}, heating experiments, pure synthetic forsterite, Fo_{100}. [k]Trull and Kurz,[22] D_{bulk}, heating experiments, olivine from Hawaiian ultramafic xenoliths, $Fo_{89.2}$. [l]Trull et al.,[60] D_{bulk}, heating experiments, olivine from Kula ankaramite. [m]Hart,[59] D_{bulk}, heating experiments, olivine from dunite xenolith.

values (e.g., from 11(6) to 77(36) kJ/mol) for grain boundary diffusion of He in polycrystalline olivine by Delon et al.[65] and the relatively low experimental temperatures (i.e., 150−600 °C), we infer that such low values may be a combination of "grain boundary" and "interstitial" mechanisms during the diffusion experiments of He in olivine like those observed by Delon et al.[65]

Additionally, our calculated ΔE_{elec} values at different pressures show unexpected deviations when compared with calculation results of Wang et al.[36] At 0 GPa, our calculated ΔE_{elec} value is slightly larger than the one from Wang et al.[36] (135.66 vs 128.33). However, such small discrepancies between ours and those of Wang et al.[36] become even more significant at 10 GPa with 234.15 versus 156.31. After detailed data analysis, we find that the main reason for such a difference is probably the choice of parameter "EDIFFG" when performing CI-NEB calculations using VASP. EDIFFG is a convergence threshold (energy or force) for the ionic relaxation loop. A negative value of EDIFFG is commonly used to control the force (eV/Å) convergence threshold during CI-NEB calculations when searching the saddle point configurations. We additionally performed a series of CI-NEB calculations for the IS → FS pathway using different settings for the "EDIFFG" parameter of −0.1, −0.02, and −0.001, while other settings are identical. Calculation results are summarized in Table 4. The results show that the value of EDIFFG can significantly affect the precision of ΔE_{elec}. With the change of EDIFFG values from −0.1 to −0.001, which indicates a stricter convergence requirement, the corresponding ΔE_{elec} values change from 129.6 to 135.7 kJ/mol. Here, the calculated ΔE_{elec} value of 129.6 kJ/mol is very close the one of 128.3 kJ/mol calculated by Wang et al.[36] with the same EDIFFG settings. Therefore, this comparison shows that it is quite necessary to increase the convergence requirement during CI-NEB calculations with proper EDIFFG settings. To obtain results with acceptable accuracy and precision, we

Table 4. Calculated ΔE_{elec} Values for IS → FS Pathway at 0 GPa with Different EDIFFG Settings of −0.1, −0.02, and −0.001[a]

EDIFFG	ΔE_{elec}(kJ/mol) this study	ΔE_{elec}(kJ/mol) Wang et al.[36]
−0.1	129.6	128.33
−0.02	136.2	
−0.001	135.7	

[a]The results of Wang et al.[36] are also listed for comparison.

used an EDIFFG value of −0.001 during our calculations. Furthermore, we also find that our calculated ΔE_{elec} slightly deviates from the fitted results for E_a of 2.1, 2.0, and 1.2 kJ/mol at 0, 10, and 20 GPa, respectively. We believe that such deviations are mainly caused by neglecting the ZPE difference between TS and IS.

4.2. DIE of He Isotopes in Forsterite: Theory Versus Experiments. A direct comparison of the DIE of He isotopes between our calculations and those previous experimental results is plotted in Figure 7 (He diffusion in vitreous silica,[67]

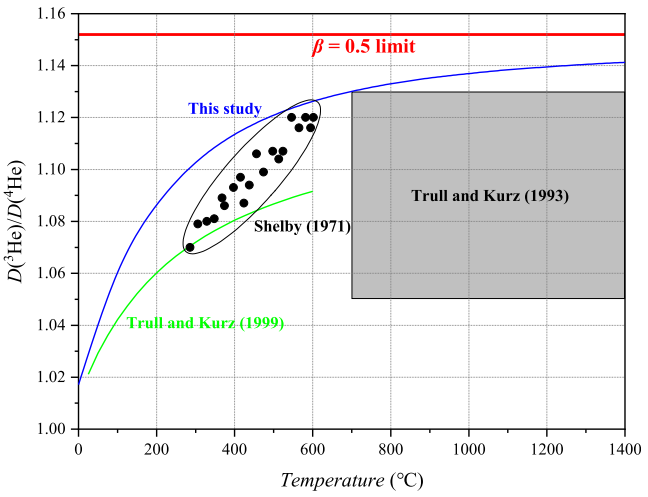

Figure 7. Comparison of results between calculated D^*/D ratios for interstitial diffusion of He isotopes in forsterite along [101] direction with previous experimental data. Data source: Shelby,[67] Trull and Kurz,[22] and Trull and Kurz.[68]

olivine,[22] and basaltic glass[68]). At temperatures from 700 to 1400 °C at 0 GPa, our results show that D^*/D ratio ranges from 0.8849 to 0.8763, corresponding to the range of D/D^* ratios from 1.130 to 1.141. These results are just close to the upper limit of 1.09 ± 0.04 obtained by Trull and Kurz[22] during their heating release experiments of He in olivine ($Fo_{89.2}$) in the same temperature range. We believe that such differences may be caused by different diffusional pathways between experiments (bulk diffusion) and calculations (interstitial diffusion along the [101] direction). In addition, these experimental results probably may represent mixed results of interstitial, vacancy, and grain boundary mechanisms and they may also be affected by other cations (e.g., Fe^{2+}) in natural olivine samples. However, the results of Trull and Kurz[22] are the only experimental data of He DIE in olivine we can find to be directly compared with so far. Compared with other experimental results, our results at 600 °C and 0 GPa (1.121) are also in good agreement with 1.120 obtained by diffusion experiments of He isotopes in vitreous silica at the same temperature.[67] Additionally, our result at 0−600 °C and 0 GPa

https://doi.org/10.1021/acsearthspacechem.2c00110
ACS Earth Space Chem. 2023, 7, 28−40

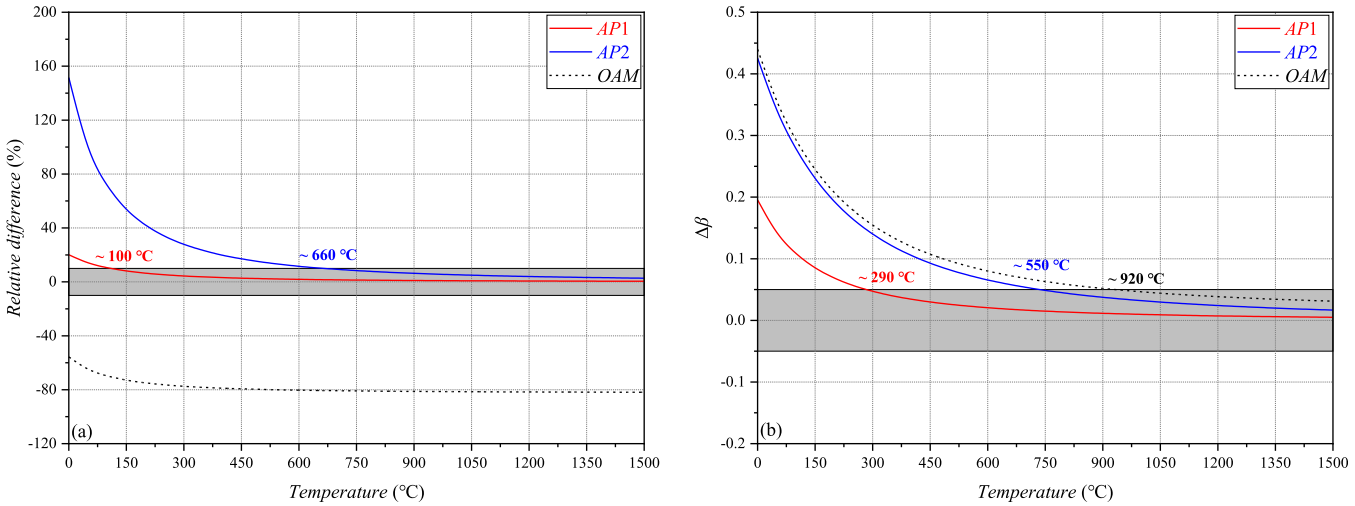

Figure 8. Calculated relative differences for Γ (a; percentage) and β values (b; deviations) obtained by AP1 and AP2 compared to these reference data obtained by eqs 9, 20, and 25. Areas in gray denote the range of deviations for Γ (±10%) and β (±0.05), respectively. All the values in the two figures show criterion temperatures when relative differences are within ±10% for Γ and ±0.05 for β. AP1 (the solid red line): eq 26. High-temperature approximation is adopted for $\nu^{\neq}$ only; AP2 (the solid blue line): eq 27. High-temperature approximation is adopted for all vibrational normal modes; OAM (the dashed black line): the one-atom model. All atoms except for the solute He atom are fixed, and only the three modes of He atom are used for calculations.

are greater than these data obtained by helium release experiments of basaltic glass samples.[68] These differences are probably caused by different He diffusion environments and pathways among our calculations and previous experiments.

4.3. Calculations of Γ and β. When it comes to the calculations of Γ and β, we have already pointed out that previous works introduced some approximations, such as the one-atom model[23,24] and the high-temperature approximation,[29] which may not be accurate enough. To further evaluate the effects of these approximations, we have calculated the Γ of ^{4}He diffusion in forsterite and corresponding β values based on our first-principles calculation results at 0 GPa from 0 to 1500 °C with all these different methods proposed in Section 2 (eqs 20, 22, and 23 for Γ and eq 25, AP1, and AP2 for β) and compared with each other. Two data sets are used: (a) all the vibrational modes of IS and TS (i.e., all-frequency model) and (b) one-atom model, that is, only the three vibrational modes directly related to the motions of the helium atom calculated by fixing all the other atoms in the system. Detailed comparisons of calculated Γ and β values are plotted in Figure 8.

For these results calculated with the all-frequency model (denoted as AP1 and AP2), Figure 8a shows that high-temperature approximation used in eq 22 will lead to more than 10% deviations compared to eq 20 at ≤~100 °C and such deviations decrease as the temperature increases. As for eq 23, it can only give reasonable results with <10% deviations at ≥~660 °C and such deviations will rapidly increase into 150% at 0 °C. At 1500 °C, both results obtained by eqs 22 and 23 have only 0.5 and 2.8% deviations compared with those of eq 20, respectively. Therefore, we believe that the high-temperature approximation condition ($h\nu \ll k_BT$) can only be safely used for calculating Γ values when the temperature is high, that is, ≥660 °C in this case (eq 23). Similar trends can also be recognized for the case of β (Figure 8b). It shows that the results of the all-frequency model will be quite close to reference values at ≥~550 °C within an error of 0.05. However, both results (AP1 and AP2) will significantly deviate from the reference values when the temperature is low (<550 °C). Therefore, it is highly recommended not to use the high-temperature approximation condition to study the DIEs at relatively low temperatures (e.g., <550 °C). On the contrary, such an approximation can be safely used for cases under high temperatures, that is, ≥~660 °C for reasonable estimations of both D and β values.

As for problems about the one-atom model,[23,24] denoted as OAM on Figure 8, our results show that the one-atom model will systematically underestimate the value of Γ with a nearly constant deviation of −80% at ≥400 °C. As for the case of β values, the one-atom model shows a behavior similar to those of the all-frequency model. According to this observation, we therefore suggest using the all-frequency model rather than the one-atom model to estimate the D values during diffusion-related theoretical studies for better accuracy. Meanwhile, the one-atom model is highly recommended to estimate DIEs at high temperatures, for example, mantle conditions.

4.4. Effects of $P\Delta V$ and ΔE_{elec}. Based on our derivations in Section 2.5, $P\Delta V$ and ΔE_{elec} items will be both canceled when calculating the D^*/D ratio under the framework of the BOA (Born and Oppenheimer[40]). However, using the fixation method for first-principles calculations will directly lead to unphysical zero values for the activation volume, which will cause serious problems for accurately estimating the D values under high pressures. Additionally, it is also quite necessary to briefly discuss the effects of adopting the BOA during our calculations.

For an atomic jump process, the migration volume ΔV is a measure of the relative size of the transition state and reactant structures.[69] Under the framework of BOA, ΔVs for different isotopes of a certain solute atom will be identical. However, things will be slightly different when beyond the BOA. A correction, so called the diagonal Born−Oppenheimer correction (DBOC), was introduced to consider such cases.[70] For example, by performing high-accuracy ab initio calculations, Valeev and Sherrill[71] found that the DBOC leads to a 0.0007 Å difference between the bond lengths of BH and BD molecules, corresponding to a 0.057% difference. In

https://doi.org/10.1021/acsearthspacechem.2c00110
ACS Earth Space Chem. 2023, 7, 28−40

addition, the energy difference between two isotopes caused by the DBOC is directly proportional to the relative mass difference ($\frac{\Delta m}{mm^*}$). Considering the relative mass difference of H/D (~50%) and ^{3}He/^{4}He (~8%), we can give an approximation of about ~0.009% difference in bond length between the ^{3}He−Mg/O and ^{4}He−Mg/O bonds in this study. Combining the ~2.0 Å bond length, we can obtain a roughly $(2.0\ \text{Å})^3 \times (1.00009^3 - 1) = 2.16 \times 10^{-33}\ \text{m}^3$, corresponding to $1.30 \times 10^{-9}\ \text{m}^3/\text{mol}$ volume difference between the ^{3}He and ^{4}He cases. For the temperature−pressure range (0−1500 °C and 0−20 GPa), such a volume difference will give an $e^{-P\Delta V/k_BT}$ factor of 0.9886−1, which can be negligible. It is the factor $e^{-P\Delta\Delta V/k_BT}$ rather than $e^{-P\Delta V/k_BT}$ that contributes to the D^*/D ratio. Therefore, we believe that at least for the DIE of the interstitial diffusion of He isotopes in forsterite, the effects of the activation volume ΔV and the PV work are quite limited, which can be safely neglected even the scenarios beyond the BOA have been considered.

As for the effect of ΔE_{elec}, Zhang and Liu[72] have analyzed the effect of the DBOC for the equilibrium isotope fractionations for H isotopes and found −4.134 to 10.716 cm^{-1} ΔE_{elec} differences among different H/D exchanged molecules. Therefore, based on these results, we can expect an approximated range of −0.7 to 1.7 cm^{-1} for He isotopes, corresponding to an $e^{-\Delta E_{elec}/k_BT}$ factor of 0.9977−1.0009. Similar to the discussions above for $P\Delta V$, the effect of the ΔE_{elec} on DIE is also limited in this study, which can be safely neglected.

Another problem about the effect of $P\Delta V$ comes from first-principles calculations as the lattice parameters of the forsterite were fixed during CI-NEB calculations.[35,36] The potential effect of such fixation on the $P\Delta V$ can be roughly estimated by external pressure difference as the small pressure difference caused by fixation will be canceled through adding non-zero external pressure during VASP calculations. We obtained that such external pressure differences are, respectively, 0.182, 0.245, and 0.229 GPa between TS and IS at 0 K under 0, 10, and 20 GPa. Inspired by the works of Vallianatos and Saltas[73] on evaluating the validity of the cBΩ model for He diffusion in olivine, we quantitatively estimate the values of ΔV and the corresponding values of $P\Delta V$ through the following ways:

(a) Assuming that the solute He atom has negligible effect on the bulk moduli (K_T) of forsterite, setting the K_T of forsterite a reasonable value of ~130 GPa[74] and combined with the third-order Birch Murnaghan equation of state with a fixed K' value of 4.0,[75] the corresponding volume at 0 K change can be calculated. ΔV (0 K) values of 4.98, 4.21, and 2.75 $Å^3$ were obtained in this way, corresponding to ΔV (0 K) values of 3.00, 2.54, and 1.66 cm^3/mol under 0, 10, and 20 GPa, respectively.

(b) ΔV values at different temperatures and pressures were estimated with the protocols proposed by Vallianatos and Saltas (eqs 15 and 16 in their study). After simple calculations, ΔV values of 3.02−3.31, 2.56−2.80, and 1.67−1.83 cm^3/mol from 0 to 1500 °C at 0, 10, and 20 GPa were obtained. We notice that our estimated ΔV at 0 GPa is slightly smaller than the previous one (3.02−3.31 vs 3.81−3.83 cm^3/mol), indicating the validity of such estimation and the robustness of our first-principles calculations indirectly.

Based on the estimation methods above, $P\Delta V$ values of 0, 25.6−28.0 and 33.4−36.6 kJ/mol are obtained from 0 to 1500 °C under 0, 10, and 20 GPa, corresponding to $e^{-P\Delta V/k_BT}$ factors of 1.0, 0.150, and 0.084 at 1500 °C. Therefore, we believe that such a fixation method is probably not applicable for accurate predictions of the Γ or D at high pressures due to the unphysical neglection of $e^{-P\Delta V/k_BT}$ item. Additionally, our calculation results only involve one certain interstitial diffusion pathway as depicted in Figure 2, that is, the IS → FS atomic jump pathway along the [101] direction, which means that this pathway is probably one of the dominant interstitial pathways for He diffusion in forsterite at 0 GPa. In other words, the dominance of the [101] pathway for interstitial diffusion of He in forsterite at high pressures is not guaranteed. Therefore, the calculated pressure effect in this study is only applicable for the [101] pathway and cannot be directly used for comparison with experimental results that are statistical averages of many different pathways with thermodynamic weights controlled by the activation energy.

However, when it comes to the DIE, we still believe that such a fixation method is applicable based on the discussions above. In other words, ignorance of the activation volume during first-principles calculations with a fixed lattice has a negligible effect on the DIE. Furthermore, we must point out that such an estimation about the effect of the fixation method on the ΔV is preliminary and semi-quantitative; much more detailed and accurate theoretical works are needed, which are far beyond the scope of this study.

5. CONCLUSIONS

The theories of the isotope effect for interstitial diffusion in solids are reviewed and improved based on quantum statistical mechanics. Combined with first-principles calculations of interstitial diffusion of He isotopes in forsterite, such a theory was tested and compared with previous works. Several conclusions are recognized and summarized below:

1. Based on the CTST and quantum statistical mechanics, we provided a unified and validated equation (eq 24) for calculating the DIE for interstitial mechanism in solids and it can be applied for any interstitial diffusion system in the future.
2. Our calculated results for D (D_0 and E_a) of He diffusion in forsterite at 0 GPa show agreements with most of experimental works.
3. Tighter convergence thresholds for CI-NEB calculations (parameter EDIFFG) are needed for accurate simulations for diffusion processes, especially processes with relatively small E_a values.
4. DIE for He isotopes in forsterite show significant temperature dependences and weak pressure dependences. Larger DIEs can be observed at higher temperatures, which is totally opposite to EIEs.
5. Our calculation results show that the one-atom model for DIE cannot provide reasonable results for Γ and β because all the information about the temperature effect on β is ignored.
6. According to our calculations, the high-temperature approximation ($h\nu \ll k_BT$) causes significant loss of accuracies for the values of D and β at low temperatures (≤660 °C for D and ≤550 °C for β). However, such an approximation method can still be safely used at higher

https://doi.org/10.1021/acsearthspacechem.2c00110
ACS Earth Space Chem. 2023, 7, 28−40

temperatures with small errors of within 10% for D and 0.05 for β.

7. The effects of $P\Delta V$ and ΔE_{elec} on β are negligible even scenarios beyond BOA are considered. However, when it comes to accurate values for D under high pressures, the effect of $P\Delta V$ cannot be ignored according to our preliminarily estimations. In other words, the commonly used fixation method (lattice parameters are fixed during CI-NEB calculations) in first-principles calculation studies may not be applicable at high pressures unless an accurate activation volume ΔV can be estimated.

■ ASSOCIATED CONTENT

Supporting Information

The Supporting Information is available free of charge at https://pubs.acs.org/doi/10.1021/acsearthspacechem.2c00110.

Derivations of eq 14, β_{ZPE}, and β_{others} (PDF)

■ AUTHOR INFORMATION

Corresponding Author

Yun Liu − *International Research Center for Planetary Science, College of Earth Sciences, Chengdu University of Technology, Chengdu 610059, China; State Key Laboratory of Ore Deposit Geochemistry, Institute of Geochemistry, Chinese Academy of Sciences, Guiyang 550081, China; CAS Center for Excellence in Comparative Planetology, Hefei 230026, China;* orcid.org/0000-0003-1000-143X; Phone: +86-13984026811; Email: liuyun@vip.gyig.ac.cn

Authors

Xuefang Li − *International Research Center for Planetary Science, College of Earth Sciences, Chengdu University of Technology, Chengdu 610059, China; State Key Laboratory of Ore Deposit Geochemistry, Institute of Geochemistry, Chinese Academy of Sciences, Guiyang 550081, China; CAS Center for Excellence in Comparative Planetology, Hefei 230026, China;* orcid.org/0000-0001-7748-3563

Yining Zhang − *State Key Laboratory of Ore Deposit Geochemistry, Institute of Geochemistry, Chinese Academy of Sciences, Guiyang 550081, China*

Complete contact information is available at: https://pubs.acs.org/10.1021/acsearthspacechem.2c00110

Author Contributions

‖X.L. and Y.Z. contributed equally to this work and should be considered co-first authors.

Notes

The authors declare no competing financial interest.

■ ACKNOWLEDGMENTS

X.L. is grateful for Chinese NSF projects (41873024, 42173021). Y.L. is grateful for funding supports from the strategic priority research program (B) of CAS (XDB41000000), pre-research Project on Civil Aerospace Technologies no. D020202 funded by Chinese National Space Administration (CNSA), and Chinese NSF projects (42130114).

■ REFERENCES

(1) Chakraborty, S. Rates and mechanisms of Fe-Mg interdiffusion in olivine at 980°-1300°C. *J. Geophys. Res.: Solid Earth* **1997**, *102*, 12317−12331.

(2) Chakraborty, S. Diffusion in Solid Silicates: A Tool to Track Timescales of Processes Comes of Age. *Earth Planet. Sci. Lett.* **2008**, *36*, 153−190.

(3) Chakraborty, S. Diffusion Coefficients in Olivine, Wadsleyite and Ringwoodite. *Rev. Mineral. Geochem.* **2010**, *72*, 603−639.

(4) Farver, J. R.; Giletti, B. J. Oxygen and strontium diffusion kinetics in apatite and potential applications to thermal history determinations. *Geochim. Cosmochim. Acta* **1989**, *53*, 1621−1631.

(5) Dodson, M. H. Closure temperature in cooling geochronological and petrological systems. *Contrib. Mineral. Petrol.* **1973**, *40*, 259−274.

(6) Ganguly, J.; Tirone, M. Diffusion closure temperature and age of a mineral with arbitrary extent of diffusion: theoretical formulation and applications. *Earth Planet. Sci. Lett.* **1999**, *170*, 131−140.

(7) Sio, C. K.; Dauphas, N.; Teng, F. Z.; Chaussidon, M.; Helz, R. T.; Roskosz, M. Discerning crystal growth from diffusion profiles in zoned olivine by in situ Mg-Fe isotopic analyses. *Geochim. Cosmochim. Acta* **2013**, *123*, 302−321.

(8) Oeser, M.; Dohmen, R.; Horn, I.; Schuth, S.; Weyer, S. Processes and time scales of magmatic evolution as revealed by Fe-Mg chemical and isotopic zoning in natural olivines. *Geochim. Cosmochim. Acta* **2015**, *154*, 130−150.

(9) Lundstrom, C. C.; Chaussidon, M.; Hsui, A. T.; Kelemen, P.; Zimmerman, M. Observations of Li isotopic variations in the Trinity Ophiolite: Evidence for isotopic fractionation by diffusion during mantle melting. *Geochim. Cosmochim. Acta* **2005**, *69*, 735−751.

(10) Teng, F. Z.; McDonough, W. F.; Rudnick, R. L.; Walker, R. J. Diffusion-driven extreme lithium isotopic fractionation in country rocks of the Tin Mountain pegmatite. *Earth Planet. Sci. Lett.* **2006**, *243*, 701−710.

(11) Parkinson, I. J.; Hammond, S. J.; James, R. H.; Rogers, N. W. High-temperature lithium isotope fractionation: Insights from lithium isotope diffusion in magmatic systems. *Earth Planet. Sci. Lett.* **2007**, *257*, 609−621.

(12) Teng, F. Z.; Rudnick, R. L.; McDonough, W. F.; Gao, S.; Tomascak, P. B.; Liu, Y. S. Lithium isotopic composition and concentration of the deep continental crust. *Chem. Geol.* **2008**, *255*, 47−59.

(13) Seitz, H. M.; Zipfel, J.; Brey, G. P.; Ott, U. Lithium isotope compositions of chondrules, CAI and a dark inclusion from Allende and ordinary chondrites. *Earth Planet. Sci. Lett.* **2012**, *329*−*330*, 51−59.

(14) Dauphas, N. Diffusion-driven kinetic isotope effect of Fe and Ni during formation of the Widmanstätten pattern. *Meteorit. Planet. Sci.* **2007**, *42*, 1597−1613.

(15) Watson, H. C.; Richter, F.; Liu, A. K.; Huss, G. R. Iron and nickel isotope fractionation by diffusion, with applications to iron meteorites. *Earth Planet. Sci. Lett.* **2016**, *451*, 159−167.

(16) Dauphas, N.; Teng, F. Z.; Arndt, N. T. Magnesium and iron isotopes in 2.7 Ga Alexo komatiites: Mantle signatures, no evidence for Soret diffusion, and identification of diffusive transport in zoned olivine. *Geochim. Cosmochim. Acta* **2010**, *74*, 3274−3291.

(17) Teng, F. Z.; Dauphas, N.; Helz, R. T.; Gao, S.; Huang, S. C. Diffusion-driven magnesium and iron isotope fractionation in Hawaiian olivine. *Earth Planet. Sci. Lett.* **2011**, *308*, 317−324.

(18) Sossi, P. A.; Nebel, O.; Foden, J. Iron isotope systematics in planetary reservoirs. *Earth Planet. Sci. Lett.* **2016**, *452*, 295−308.

(19) Sio, C. K. I.; Dauphas, N. Thermal and crystallization histories of magmatic bodies by Monte Carlo inversion of Mg-Fe isotopic profiles in olivine. *Geology* **2017**, *45*, 67−70.

(20) Sio, C. K.; Roskosz, M.; Dauphas, N.; Bennett, N. R.; Mock, T.; Shahar, A. The isotope effect for Mg-Fe interdiffusion in olivine and its dependence on crystal orientation, composition and temperature. *Geochim. Cosmochim. Acta* **2018**, *239*, 463−480.

(21) Eyring, H. The Activated Complex in Chemical Reactions. *J. Chem. Phys.* **1935**, *3*, 107−115.

(22) Trull, T. W.; Kurz, M. D. Experimental measurements of ^{3}He and ^{4}He mobility in olivine and clinopyroxene at magmatic temperatures. *Geochim. Cosmochim. Acta* **1993**, *57*, 1313−1324.
(23) Wert, C.; Zener, C. Interstitial atomic diffusion coefficients. *Phys. Rev.* **1949**, *76*, 1169−1175.
(24) Wert, C. A. Diffusion Coefficient of C in α-Iron. *Phys. Rev.* **1950**, *79*, 601−605.
(25) Vineyard, G. H. Frequency factors and isotope effects in solid state rate processes. *J. Phys. Chem. Solids* **1957**, *3*, 121−127.
(26) Schoen, A. H. Correlation and the Isotope Effect for Diffusion in Crystalline Solids. *Phys. Rev. Lett.* **1958**, *1*, 138−140.
(27) Tharmalingam, K.; Lidiard, A. B. Isotope effect in vacancy diffusion. *Philos. Mag.* **1959**, *4*, 899−906.
(28) Mullen, J. G. Isotope Effect in Intermetallic Diffusion. *Phys. Rev.* **1961**, *121*, 1649−1658.
(29) Le Claire, A. D. Some comments on the mass effect in diffusion. *Philos. Mag.* **1966**, *14*, 1271−1284.
(30) Dominguez, G.; Wilkins, G.; Thiemens, M. H. The Soret effect and isotopic fractionation in high-temperature silicate melts. *Nature* **2011**, *473*, 70−73.
(31) Li, X. F.; Liu, Y. A theoretical model of isotopic fractionation by thermal diffusion and its implementation on silicate melts. *Geochim. Cosmochim. Acta* **2015**, *154*, 18−27.
(32) Van Orman, J. A.; Krawczynski, M. J. Theoretical constraints on the isotope effect for diffusion in minerals. *Geochim. Cosmochim. Acta* **2015**, *164*, 365−381.
(33) Ammann, M. W.; Brodholt, J. P.; Dobson, D. P. DFT study of migration enthalpies in $MgSiO_3$ perovskite. *Phys. Chem. Miner.* **2008**, *36*, 151−158.
(34) Ammann, M. W.; Brodholt, J. P.; Wookey, J.; Dobson, D. P. First-principles constraints on diffusion in lower-mantle minerals and a weak D″ layer. *Nature* **2010**, *465*, 462−465.
(35) Bengtson, A.; Ewing, R. C.; Becker, U. He diffusion and closure temperatures in apatite and zircon: A density functional theory investigation. *Geochim. Cosmochim. Acta* **2012**, *86*, 228−238.
(36) Wang, K.; Brodholt, J. P.; Lu, X. C. Helium diffusion in olivine based on first principles calculations. *Geochim. Cosmochim. Acta* **2015**, *156*, 145−153.
(37) Wang, K.; Lu, X. C.; Brodholt, J. P. Diffusion of noble gases in subduction zone hydrous minerals. *Geochim. Cosmochim. Acta* **2020**, *291*, 50−61.
(38) Mehrer, H.*Diffusion in Solids: Fundamentals, Methods, Methods, Materials, Diffusion-Controlled Process*; Spring Berlin Heidelberg: New York, 2007.
(39) Leclaire, A. D.; Lidiard, A. B. LIII. Correlation effects in diffusion in crystals. *Philos. Mag.* **1956**, *1*, 518−527.
(40) Born, M.; Oppenheimer, R.On the quantum theory of molecules. *Quantum Chemistry: Classic Scientific Papers*; World Scientific, 1927.
(41) Jambon, A. Isotopic fractionation: A kinetic model for crystals growing from magmatic melts. *Geochim. Cosmochim. Acta* **1980**, *44*, 1373−1380.
(42) Tsuchiyama, A.; Kawamura, K.; Nakao, T.; Uyeda, C. Isotopic effects on diffusion in MgO melt simulated by the molecular dynamics (MD) method and implications for isotopic mass fractionation in magmatic systems. *Geochim. Cosmochim. Acta* **1994**, *58*, 3013−3021.
(43) Richter, F. M.; Davis, A. M.; DePaolo, D. J.; Watson, E. B. Isotope fractionation by chemical diffusion between molten basalt and rhyolite. *Geochim. Cosmochim. Acta* **2003**, *67*, 3905−3923.
(44) Richter, F. M.; Liang, Y.; Davis, A. M. Isotope fractionation by diffusion in molten oxides. *Geochim. Cosmochim. Acta* **1999**, *63*, 2853−2861.
(45) Goel, G.; Zhang, L. Q.; Lacks, D. J.; Van Orman, J. A. Isotope fractionation by diffusion in silicate melts: Insights from molecular dynamics simulations. *Geochim. Cosmochim. Acta* **2012**, *93*, 205−213.
(46) Bigeleisen, J.; Wolfsberg, M.Theoretical and Experimental Aspects of Isotope Effects in Chemical Kinetics. *Advances in Chemical Physics*; John Wiley & Sons, Inc., 1958.
(47) Kamakoti, P.; Sholl, D. S. Ab initio lattice-gas modeling of interstitial hydrogen diffusion in CuPd alloys. *Phys. Rev. B: Condens. Matter Mater. Phys.* **2005**, *71*, 014301.
(48) Koettgen, J.; Zacherle, T.; Grieshammer, S.; Martin, M. Ab initio calculation of the attempt frequency of oxygen diffusion in pure and samarium doped ceria. *Phys. Chem. Chem. Phys.* **2017**, *19*, 9957−9973.
(49) Song, Z. W.; Wu, H.; Shu, S. P.; Krawczynski, M.; Van Orman, J.; Cherniak, D. J.; Bruce Watson, E. B.; Mukhopadhyay, S.; Morgan, D. A first-principles and experimental study of helium diffusion in periclase MgO. *Phys. Chem. Miner.* **2018**, *45*, 641−654.
(50) Kresse, G.; Hafner, J. Ab initiomolecular dynamics for liquid metals. *Phys. Rev. B: Condens. Matter Mater. Phys.* **1993**, *47*, 558−561.
(51) Kresse, G.; Furthmüller, J. Efficiency of ab-initio total energy calculations for metals and semiconductors using a plane-wave basis set. *Comput. Mater. Sci.* **1996**, *6*, 15−50.
(52) Henkelman, G.; Jónsson, H. Improved tangent estimate in the nudged elastic band method for finding minimum energy paths and saddle points. *J. Chem. Phys.* **2000**, *113*, 9978−9985.
(53) Henkelman, G.; Uberuaga, B. P.; Jónsson, H. A climbing image nudged elastic band method for finding saddle points and minimum energy paths. *J. Chem. Phys.* **2000**, *113*, 9901−9904.
(54) Henkelman, G.; Jóhannesson, G.; Jónsson, H.Methods for Finding Saddle Points and Minimum Energy Paths. In *Theoretical Methods in Condensed Phase Chemistry*; Schwartz, S. D., Ed.; Springer Netherlands: Dordrecht, 2002; pp 269−302.
(55) Blöchl, P. E. Projector augmented-wave method. *Phys. Rev. B: Condens. Matter Mater. Phys.* **1994**, *50*, 17953−17979.
(56) Kresse, G.; Joubert, D. From ultrasoft pseudopotentials to the projector augmented-wave method. *Phys. Rev. B: Condens. Matter Mater. Phys.* **1999**, *59*, 1758−1775.
(57) Perdew, J. P.; Wang, Y. Accurate and simple analytic representation of the electron-gas correlation energy. *Phys. Rev. B: Condens. Matter Mater. Phys.* **1992**, *45*, 13244−13249.
(58) Fujino, K.; Sasaki, S.; Takéuchi, Y.; Sadanaga, R. X-ray determination of electron distributions in forsterite, fayalite and tephroite. *Acta Crystallogr.* **1981**, *37*, 513−518.
(59) Hart, S. R. He diffusion in olivine. *Earth Planet. Sci. Lett.* **1984**, *70*, 297−302.
(60) Trull, T. W.; Kurz, M. D.; Jenkins, W. J. Diffusion of cosmogenic ^{3}He in olivine and quartz - Implications for surface exposure dating. *Earth Planet. Sci. Lett.* **1991**, *103*, 241−256.
(61) Futagami, T.; Ozima, M.; Nagal, S.; Aoki, Y. Experiments on thermal release of implanted noble gases from minerals and their implications for noble gases in lunar soil grains. *Geochim. Cosmochim. Acta* **1993**, *57*, 3177−3194.
(62) Shuster, D. L.; Farley, K. A.; Sisterson, J. M.; Burnett, D. S. Quantifying the diffusion kinetics and spatial distributions of radiogenic ^{4}He in minerals containing proton-induced ^{3}He. *Earth Planet. Sci. Lett.* **2004**, *217*, 19−32.
(63) Blard, P. H.; Puchol, N.; Farley, K. A. Constraints on the loss of matrix-sited helium during vacuum crushing of mafic phenocrysts. *Geochim. Cosmochim. Acta* **2008**, *72*, 3788−3803.
(64) Tolstikhin, I.; Kamensky, I.; Tarakanov, S.; Kramers, J.; Pekala, M.; Skiba, V.; Gannibal, M.; Novikov, D. Noble gas isotope sites and mobility in mafic rocks and olivine. *Geochim. Cosmochim. Acta* **2010**, *74*, 1436−1447.
(65) Delon, R.; Demouchy, S.; Marrocchi, Y.; Bouhifd, M. A.; Barou, F.; Cordier, P.; Addad, A.; Burnard, P. G. Helium incorporation and diffusion in polycrystalline olivine. *Chem. Geol.* **2018**, *488*, 105−124.
(66) Cherniak, D. J.; Watson, E. B. Diffusion of helium in olivine at 1 atm and 2.7 GPa. *Geochim. Cosmochim. Acta* **2012**, *84*, 269−279.
(67) Shelby, J. E. Diffusion of helium isotopes in vitreous silica. *Phys. Rev. B: Solid State* **1971**, *4*, 2681−2686.
(68) Trull, T. W.; Kurz, M. D. Isotopic fractionation accompanying helium diffusion in basaltic glass. *J. Mol. Struct.* **1999**, *485*−*486*, 555−567.
(69) Piskulich, Z. A.; Mesele, O. O.; Thompson, W. H. Activation Energies and Beyond. *J. Phys. Chem. A* **2019**, *123*, 7185−7194.

(70) Born, M.; Huang, K.*Dynamical Theory of Crystal Lattices*; Oxford University: New York, 1956.
(71) Valeev, E. F.; Sherrill, C. D. The diagonal Born-Oppenheimer correction beyond the Hartree-Fock approximation. *J. Chem. Phys.* **2003**, *118*, 3921−3927.
(72) Zhang, Y. N.; Liu, Y. The theory of equilibrium isotope fractionations for gaseous molecules under super-cold conditions. *Geochim. Cosmochim. Acta* **2018**, *238*, 123−149.
(73) Vallianatos, F.; Saltas, V. Application of the cBΩ model to the calculation of diffusion parameters of He in olivine. *Phys. Chem. Miner.* **2014**, *41*, 181−188.
(74) Finkelstein, G. J.; Dera, P. K.; Jahn, S.; Oganov, A. R.; Holl, C. M.; Meng, Y.; Duffy, T. S. Phase transitions and equation of state of forsterite to 90 GPa from single-crystal X-ray diffraction and molecular modeling. *Am. Mineral.* **2014**, *99*, 35−43.
(75) Birch, F. Finite elastic strain of cubic crystals. *Phys. Rev.* **1947**, *71*, 809−824.

https://doi.org/10.1021/acsearthspacechem.2c00110
ACS Earth Space Chem. 2023, 7, 28−40